Materials Science & Engineering A 639 (2015) 345–349

Contents lists available at ScienceDirect

Materials Science & Engineering A

journal homepage: www.elsevier.com/locate/msea

Effect of Ti addition on the glass forming ability, crystallization, and plasticity of $(Zr_{64.13}Cu_{15.75}Ni_{10.12}Al_{10})_{100-x}Ti_x$ bulk metallic glasses

Bo Shi, Yuanli Xu, Wenli Ma, Chao Li, Carmen Verge Estefania, Jiangong Li*

Institute of Materials Science and Engineering and MOE Key Laboratory for Magnetism and Magnetic Materials, Lanzhou University, Lanzhou 730000, China

ARTICLE INFO

Article history:
Received 26 January 2015
Received in revised form
25 April 2015
Accepted 28 April 2015
Available online 8 May 2015

Keywords:
Bulk metallic glass
Minor addition
Glass forming ability
Crystallization behavior
Plasticity

ABSTRACT

A series of $(Zr_{64.13}Cu_{15.75}Ni_{10.12}Al_{10})_{100-x}Ti_x$ (x=0–7) bulk metallic glasses were prepared by water-cooled copper mold casting method. The glass forming ability, crystallization behavior, and plasticity of the $(Zr_{64.13}Cu_{15.75}Ni_{10.12}Al_{10})_{100-x}Ti_x$ alloys with different Ti contents were studied. The reduced glass transition temperature increases with Ti addition and a maximum value of 0.562 is achieved at x=5, indicating that the glass forming ability increases with Ti addition. Compared with that of one crystallization step for the sample without Ti addition, the Ti ($x \geq 2$) containing alloys exhibit a two-step crystallization behavior. In addition, the initial crystallization temperature decreases from 744 to 684 K as x increases from 0 to 7. Icosahedral quasicrystal phase was found to precipitate in the amorphous matrix in the first crystallization step, implying that strong icosahedral short-range order may exist in the Ti ($x \geq 2$) containing alloys. Moreover, the $(Zr_{64.13}Cu_{15.75}Ni_{10.12}Al_{10})_{100-x}Ti_x$ bulk metallic glasses exhibit excellent plasticity, i.e., a plastic engineering strain in compression larger than 80% for $x \leq 6$.

1. Introduction

Bulk metallic glasses (BMGs) have attracted increasing interest in recent years due to their unique properties such as high strength, large elastic limit, excellent soft magnetic properties, and good corrosion resistance [1–3]. However, the deformation of BMGs at room temperature is highly localized into shear bands and usually propagates rapidly due to work softening [4–6], resulting in catastrophic failure along a single shear band and a limited plastic strain for BMGs. Therefore, their application as structural material is limited severely by their poor room-temperature plasticity. To overcome the intrinsic brittleness of BMGs, different approaches including in-situ or ex-situ introduction of a second crystalline phase into the glassy matrix [7,8], enhancing the Poisson's ratio [9], and heterogeneous structure [10] have been developed. All of these approaches can be easily achieved by means of minor element addition. Minor element addition has also been found to have dramatic effects on the glass forming ability (GFA), structure, and the improvement of properties of BMGs [11,12]. Hence, it seems that minor addition can be used as a promising way to explore new BMG systems with outstanding mechanical properties in conjunction with high GFA.

Recently, based on Inoue's $Zr_{65}Cu_{15}Ni_{10}Al_{10}$ BMG, which shows a very limited compressive plastic strain (2.22%) [13,14], Liu et al. slightly adjusted the composition and obtained a $Zr_{64.13}Cu_{15.75}Ni_{10.12}Al_{10}$ quaternary system with excellent room-temperature plasticity, i.e., a high compression plastic strain of more than 80% [15]. Liu et al.'s work mentioned here indicates that the plasticity of Zr–Cu–Ni–Al BMGs is very sensitive to their composition. For a plastic metallic glass system, it is obviously very important to widen the range of its composition as much as possible without losing its original plasticity. In this case, other preferable properties such as a better GFA may be obtained. It is obviously significant to broaden the potential applications of this BMG system. In this respect, minor element addition is probably an effective and interesting way to widen the composition of metallic glasses [16].

A variety of elements have been chosen as additions to metallic glasses, among which Ti is a good candidate. Especially for Cu and Zr based metallic glasses, Ti has shown significant effects on the improvement of the GFA and properties of the glassy alloys [17–21]. For example, compared with the $Zr_{65}Al_{7.5}Cu_{27.5}$ alloy with some crystalline phases in the amorphous matrix, $(Zr_{65}Al_{7.5}Cu_{27.5})_{100-x}Ti_x$ alloys with fully amorphous structure were obtained. This indicates that the GFA of $Zr_{65}Al_{7.5}Cu_{27.5}$ alloy was enhanced by Ti addition [20]. In addition, the plastic strain of a Cu–Zr–Al metallic glass increased from 1.5% to 32.5% by the introduction of minor Ti [18]. Moreover, the structure (the short range order) as well as the crystallization behavior of a Zr–Cu–Ni–Al metallic glass was changed by the addition of Ti [22,23]. In summary, Ti is an effective minor addition element to improve the GFA and mechanical properties of Cu and Zr based metallic glasses. As mentioned above, there are undoubtedly interesting potential applications for $Zr_{64.13}Cu_{15.75}Ni_{10.12}Al_{10}$ metallic

* Corresponding author. Fax.: +86 931 8910364.
E-mail address: lijg@lzu.edu.cn (J. Li).

http://dx.doi.org/10.1016/j.msea.2015.04.100
0921-5093/

glass with excellent plasticity. However, the plasticity of this metallic glass system is very sensitive to its composition. Moreover, the GFA of this metallic glass system seems relatively low. Hence, theoretically speaking, it is obviously very important to widen the range of its composition and increase its GFA without losing its original plasticity. Ti seems a good choice to be added to $Zr_{64.13}Cu_{15.75}Ni_{10.12}Al_{10}$ metallic glass, which has not been reported yet.

In this work, starting with the $Zr_{64.13}Cu_{15.75}Ni_{10.12}Al_{10}$ metallic glass system with excellent plasticity, $(Zr_{64.13}Cu_{15.75}Ni_{10.12}Al_{10})_{100-x}Ti_x$ BMGs with different Ti contents ($x=0$–7) were obtained. The effect of Ti addition on the GFA, crystallization behavior, and plasticity of $(Zr_{64.13}Cu_{15.75}Ni_{10.12}Al_{10})_{100-x}Ti_x$ BMGs have been studied.

2. Experimental

$Zr_{64.13}Cu_{15.75}Ni_{10.12}Al_{10}$ ingots were prepared by arc-melting the mixtures of Zr (99.8%), Cu (99.99%), Ni (99.99%), and Al (99.99%) elements in Ti-gettered argon atmosphere. Then $(Zr_{64.13}Cu_{15.75}Ni_{10.12}Al_{10})_{100-x}Ti_x$ ($x=0$–7) ingots were prepared by arc-melting the as-prepared $Zr_{64.13}Cu_{15.75}Ni_{10.12}Al_{10}$ ingots with Ti (99.99%) under the same conditions. Each ingot was remelted more than six times to ensure the compositional homogeneity and suction-casted into a water cooled copper mold. The $(Zr_{64.13}Cu_{15.75}Ni_{10.12}Al_{10})_{100-x}Ti_x$ rods with a length of 70 mm were obtained in two different shapes: a cylinder with a diameter of 4 mm and a bar with a square cross section of 2×2 mm^2. The structure of the as-cast samples was investigated by X-ray diffraction (XRD) with a Rigaku D/max-2400 X-ray diffractometer with Cu K_α radiation and high resolution transmission electron microscopy (HRTEM) on a FEI Tecnai G2 F30 electron microscope operating at 300 kV. The thermal response of each sample was analyzed by differential scanning calorimetry (DSC) and differential thermal analysis (DTA) on a Perkin-Elmer Pyris Diamond thermal analyzer under a continuous argon flow at a heating rate of 20 K/min. The compression tests were performed using a universal testing machine (WDW-100D, China). The specimens with a square cross section of 2×2 mm^2 and a length of 4 mm were cut from the as-cast bar and used for the compression tests at a strain rate of 1×10^{-3} s^{-1}. Before compression, these specimens were carefully polished to ensure good parallelity between the top and bottom end planes. The shear band patterns on the side surface of the deformed samples were analyzed by scanning electron microscopy (SEM) using a Hitachi S-4800 field emission scanning electron microscope operating at an acceleration voltage of 5 kV.

3. Results and discussion

The XRD patterns of the as-cast $(Zr_{64.13}Cu_{15.75}Ni_{10.12}Al_{10})_{100-x}Ti_x$ ($x=0$–7) samples with a square cross section of 2×2 mm^2 are shown in Fig. 1. The samples with Ti contents from $x=0$–7 all exhibit only a broad diffuse halo around $2\theta=36.8°$. No detectable sharp diffraction peak corresponding to any crystalline phases was observed. This reveals the amorphous nature of the as-cast samples.

To investigate the structure of the as-cast $(Zr_{64.13}Cu_{15.75}Ni_{10.12}Al_{10})_{100-x}Ti_x$ ($x=0$–7) samples further, HRTEM observations and selected area electron diffraction (SAED) analyses were performed. The corresponding HRTEM image and the SAED patterns of the as-cast $(Zr_{64.13}Cu_{15.75}Ni_{10.12}Al_{10})_{100-x}Ti_x$ samples with $x=5$ and 7 are shown in Fig. 2. For the sample with $x=5$, a homogenous maze pattern can be observed (Fig. 2(a)). In addition, the corresponding SAED pattern shown in the inset of Fig. 2(a) consists of a broad diffraction halo and a faint larger one. Hence, the as-cast $(Zr_{64.13}Cu_{15.75}Ni_{10.12}Al_{10})_{100-x}Ti_x$ sample with $x=5$ is completely amorphous.

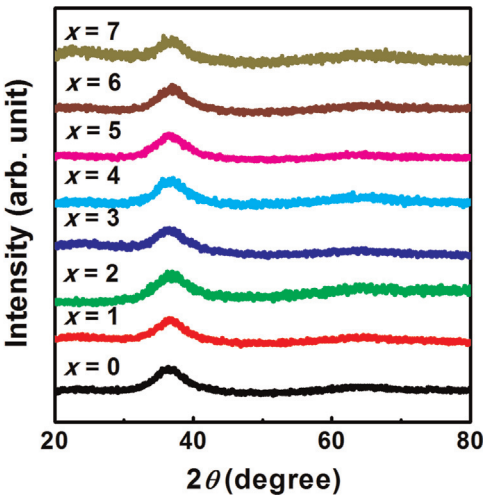

Fig. 1. The XRD patterns of the as-cast $(Zr_{64.13}Cu_{15.75}Ni_{10.12}Al_{10})_{100-x}Ti_x$ samples ($x=0$–7).

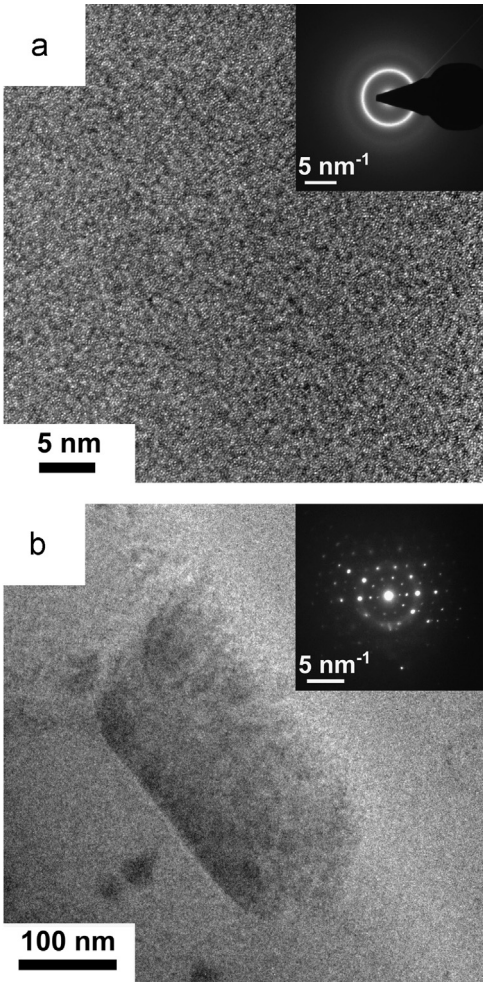

Fig. 2. (a) The HRTEM image and the corresponding SAED pattern of the as-cast sample with $x=5$. (b) The bright-field TEM image and the corresponding SAED pattern of the as-cast sample with $x=7$.

The corresponding HRTEM and SAED results (not shown) for the as-cast $(Zr_{64.13}Cu_{15.75}Ni_{10.12}Al_{10})_{100-x}Ti_x$ samples with $x=0$, 1, 2, 3, 4, and 6 are similar to that for the sample with $x=5$, indicating that the as-cast $(Zr_{64.13}Cu_{15.75}Ni_{10.12}Al_{10})_{100-x}Ti_x$ samples with $x\leq6$ are all amorphous. However, for the sample with $x=7$, some particles

embedded in the matrix can be observed, as shown in Fig. 2(b). The SAED pattern (the inset in Fig. 2(b)) consists of a broad diffraction halo and some five-fold symmetry diffraction spots. This indicates that for the sample with the Ti addition of $x=7$, some icosahedral quasicrystal phase formed in the glassy matrix.

To investigate the influence of Ti addition on the related thermal parameters of $(Zr_{64.13}Cu_{15.75}Ni_{10.12}Al_{10})_{100-x}Ti_x$ bulk metallic glasses, DSC and DTA measurements were performed at 20 K/min heating rate. The DSC traces of the as-cast $(Zr_{64.13}Cu_{15.75}Ni_{10.12}Al_{10})_{100-x}Ti_x$ samples with $x=0$–7 are plotted in Fig. 3. From Fig. 3 it can be seen that the as-cast $(Zr_{64.13}Cu_{15.75}Ni_{10.12}Al_{10})_{100-x}Ti_x$ sample without Ti addition ($x=0$) exhibits a broad endothermic event due to the glass transition and the corresponding glass transition temperature T_g (defined as the onset of the corresponding endothermic event) is about 641 K. In addition, only one crystallization event can be seen from the DSC curve for the sample without Ti addition ($x=0$) and the initial crystallization temperature T_x is about 744 K. The DSC curve for the as-cast $(Zr_{64.13}Cu_{15.75}Ni_{10.12}Al_{10})_{100-x}Ti_x$ sample with $x=1$ is similar to that for the sample without Ti addition, i.e., exhibiting a glass transition and a one-step crystallization event. For the as-cast $(Zr_{64.13}Cu_{15.75}Ni_{10.12}Al_{10})_{100-x}Ti_x$ samples with $x=2$–7, the glass transition temperature remains almost the same as that for the samples with $x=0$ and 1. However, two crystallization events can be clearly observed for the samples with $x=2$–7. To demonstrate clearly the influence of Ti addition on the thermal parameters of the $(Zr_{64.13}Cu_{15.75}Ni_{10.12}Al_{10})_{100-x}Ti_x$ samples, some parameters derived from the DSC curves shown in Fig. 3 as well as the liquidus temperature T_l determined from DTA measurement are listed in Table 1. As can be clearly seen from Table 1, the glass transition temperature

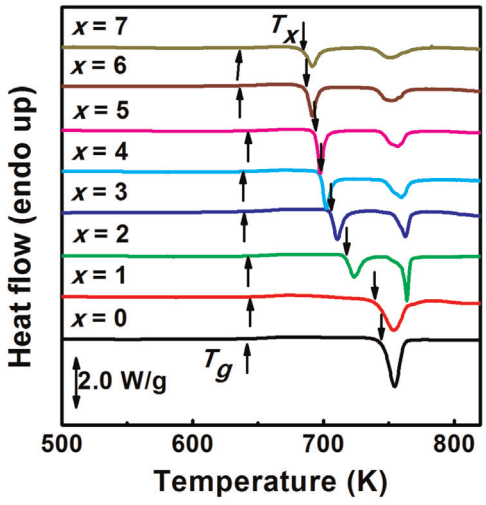

Fig. 3. The DSC traces of the as-cast samples with different Ti contents x.

Table 1
Thermal analysis data of the as-cast $(Zr_{64.13}Cu_{15.75}Ni_{10.12}Al_{10})_{100-x}Ti_x$ samples with different Ti contents x: the glass transition temperature (T_g), the onset temperature of the first crystallization event (T_x), the enthalpy of the first crystallization event (ΔH_1), the liquidus temperature (T_l), and the reduced glass transition temperature ($T_{rg}= T_g/T_l$).

x	T_g (K)	T_x (K)	ΔH_1 (J/g)	T_l (K)	T_{rg}
0	641	744	–	1164	0.551
1	644	739	–	1161	0.555
2	643	717	26.64	1157	0.556
3	639	705	27.24	1149	0.556
4	637	697	27.51	1148	0.555
5	642	693	29.94	1142	0.562
6	636	685	26.85	1138	0.559
7	635	684	24.61	1135	0.559

T_g slightly changes with Ti addition and the initial crystallization temperature T_x decreases from 744 K to 684 K as the Ti content x increases from 0 to 7. It is well known that the reduced glass transition temperature $T_{rg}= T_g/T_l$ is a good indicator reflecting the GFA of metallic glasses [24]. From Table 1, the liquidus temperature T_l decreases monotonously from 1164 K for the sample without Ti addition to 1135 K for the sample with a Ti content of $x=7$. Hence T_{rg} increases with Ti addition, which indicates that the GFA is enhanced by Ti addition for the $(Zr_{64.13}Cu_{15.75}Ni_{10.12}Al_{10})_{100-x}Ti_x$ alloys. The enthalpy of the first crystallization event ΔH_1 is basically independent of the Ti content for x increasing from 0 to 6. The value of ΔH_1 decreases suddenly at $x=7$. This can probably be attributed to the precipitation of icosahedral quasicrystal phase in the alloy, as observed by TEM (Fig. 2(b)).

To further confirm that the GFA increases with Ti addition, the as-cast $(Zr_{64.13}Cu_{15.75}Ni_{10.12}Al_{10})_{100-x}Ti_x$ ($x=0$ and 5) samples rods with diameter of 4 mm were examined by XRD and the results are shown in Fig. 4. As can be seen, the XRD pattern for the sample with $x=5$ exhibits a broad diffuse halo around $2\theta=36.8°$. This reveals that the as-cast $(Zr_{64.13}Cu_{15.75}Ni_{10.12}Al_{10})_{100-x}Ti_x$ sample of 4 mm in diameter with $x=5$ has fully amorphous structure. However, the XRD pattern for the as-cast $(Zr_{64.13}Cu_{15.75}Ni_{10.12}Al_{10})_{100-x}Ti_x$ sample of 4 mm in diameter without Ti addition ($x=0$) exhibits clear diffraction peaks corresponding to crystalline phases. Obviously, the critical diameter of Ti-containing sample ($x=5$) is larger than that of the Ti-free sample. Conclusively, the increase of T_{rg} as well as the XRD results shown here reveal that the GFA of $(Zr_{64.13}Cu_{15.75}Ni_{10.12}Al_{10})_{100-x}Ti_x$ alloys is increased by Ti addition.

As mentioned previously, the crystallization processes changed from a one-step to a two-step behavior for the as-cast $(Zr_{64.13}Cu_{15.75}Ni_{10.12}Al_{10})_{100-x}Ti_x$ samples with $x \geq 2$, and the reason may be attributed to the variation of the short range order caused by the Ti element [22,23]. The change of short range order can further alter the phase transformation products of metallic glasses [22,23]. Hence, it is necessary to clarify the phase transformation products of the related crystallization events. For this purpose, the as-cast $(Zr_{64.13}Cu_{15.75}Ni_{10.12}Al_{10})_{100-x}Ti_x$ sample with $x=5$ was heated from room temperature up to the end temperature of the first crystallization event (703 K) and then cooled naturally. Subsequently, XRD examination was performed to determine the products formed during the first crystallization process. The corresponding XRD pattern shown in Fig. 5 consists of an intense double peak and several weak peaks. On the basis of previous reports and the indexing scheme of Bancel [22,25], the product of the first crystallization event for the as-cast $(Zr_{64.13}Cu_{15.75}Ni_{10.12}Al_{10})_{100-x}Ti_x$ sample with $x=5$ was identified as icosahedral quasicrystal phase. The formation

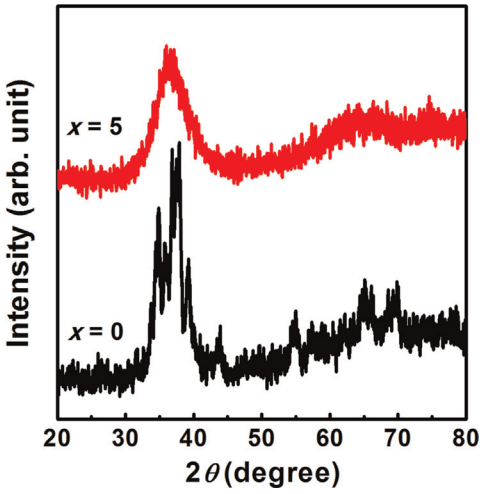

Fig. 4. The XRD patterns of the as-cast $x=0$ and $x=5$ samples of 4 mm diameter.

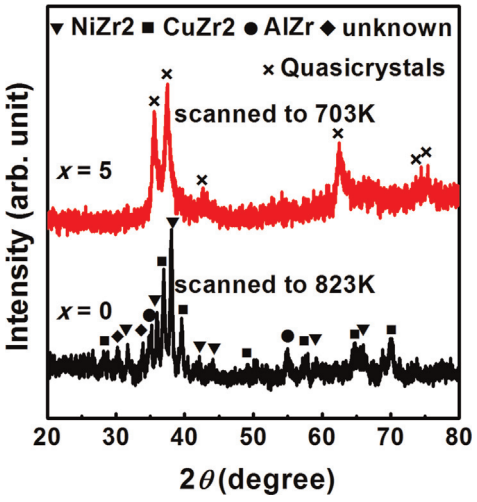

Fig. 5. The XRD patterns of the samples with $x=0$ and 5 after heated at 823 and 703 K, respectively.

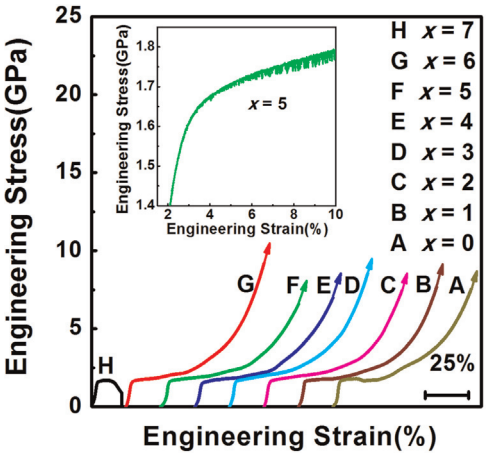

Fig. 6. The room-temperature compressive engineering stress–strain curves of the as-cast samples with $x=0$–7. The inset shows a part of the engineering stress–strain curve of the sample with $x=5$.

of icosahedral quasicrystals in the first crystallization process suggests the existence of strong icosahedral short-range order (ISRO) clusters in amorphous phase [22]. To compare with the product of the first crystallization process for the sample with $x=5$, the as-cast $(Zr_{64.13}Cu_{15.75}Ni_{10.12}Al_{10})_{100-x}Ti_x$ sample with $x=0$ was also heated from room temperature up to 823 K and then cooled naturally. The crystallization products were also checked by XRD (Fig. 5). It was found that the crystallization products for the as-cast $(Zr_{64.13}Cu_{15.75}Ni_{10.12}Al_{10})_{100-x}Ti_x$ sample with $x=0$ correspond to $NiZr_2$, $CuZr_2$, and AlZr intermetallic compounds. Hence, the short range order of the $Zr_{64.13}Cu_{15.75}Ni_{10.12}Al_{10}$ metallic glass was changed by Ti addition. This may be the possible reason for the change of the crystallization behavior and the corresponding crystallization products for the $(Zr_{64.13}Cu_{15.75}Ni_{10.12}Al_{10})_{100-x}Ti_x$ metallic glasses with Ti addition.

To investigate the influence of Ti addition on the plasticity of $(Zr_{64.13}Cu_{15.75}Ni_{10.12}Al_{10})_{100-x}Ti_x$ metallic glasses, the samples were deformed by compression tests at a strain rate of $1\times10^{-3}\,s^{-1}$. Fig. 6 shows the room-temperature compression stress–strain curves of the as-cast $(Zr_{64.13}Cu_{15.75}Ni_{10.12}Al_{10})_{100-x}Ti_x$ samples with $x=0$–7. As can be seen, all the samples with Ti contents $x<7$ exhibit a super large engineering plastic strain, larger than 80%, at room temperature. However, the sample with $x=7$ fails already at 15% strain. The decrease of plasticity may be attributed to the precipitation of icosahedral quasicrystals from the glassy matrix if the Ti addition is higher than $x=6$, as observed by TEM (Fig. 2(b)). For the sample with $x=5$, a typical serrated flow was observed, as shown in the inset of Fig. 6. The super large engineering plastic strain for the samples with $x=2$–6 may be attributed to the existence of strong ISRO in amorphous phase [22], which causes a heterogeneous structure in the as-cast samples. Moreover, it was found that dense multiple shear bands formed on the lateral surface of the sample with $x=5$ (Fig. 7(a) and (b)). This reveals that the sample undergoes severe deformation. Hence, the samples with Ti contents $x\le6$ exhibit excellent plasticity.

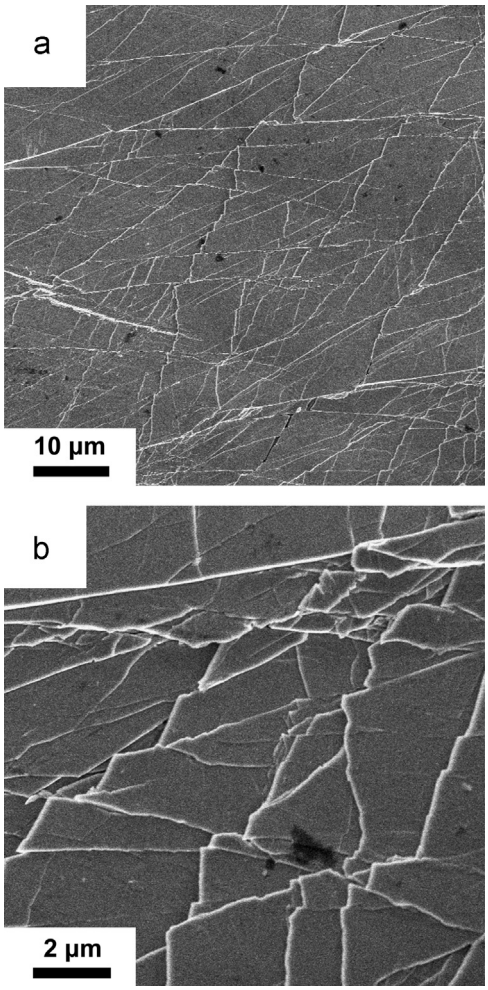

Fig. 7. The SEM micrographs of the side surface of the sample with $x=5$ after deformation to 80% compression engineering strain (a, b).

4. Conclusions

The reduced glass transition temperature increases with Ti addition and a maximum value of 0.562 is achieved at $x=5$. In addition, compared with the existence of crystalline phases in the as-cast $(Zr_{64.13}Cu_{15.75}Ni_{10.12}Al_{10})_{100-x}Ti_x$ sample of 4 mm in diameter without Ti addition, full amorphous structure is obtained for the sample of 4 mm in diameter with $x=5$. These results indicate that the addition of Ti increases the GFA of the $(Zr_{64.13}Cu_{15.75}Ni_{10.12}Al_{10})_{100-x}Ti_x$ ($x=0$–7) BMGs. Compared with the sample without Ti addition, the crystallization behavior of the $(Zr_{64.13}Cu_{15.75}Ni_{10.12}Al_{10})_{100-x}Ti_x$ ($x\ge2$) BMGs changes from a one-step to a two-step behavior. In the samples with $x\ge2$, icosahedral quasicrystals form in the first crystallization step, indicating that strong ISRO clusters may

exist in these metallic glass samples already in the as-cast state. Moreover, the excellent plasticity is retained, i.e., a large plastic engineering strain ($>80\%$) is attained for the samples with Ti addition ($x \leq 6$), which may be attributed to the existence of ISRO clusters existing in the amorphous matrix in these samples.

Acknowledgment

This work was supported by the National Natural Science Foundation of China (51071079, 51272098, and 51301080).

References

[1] A.L. Greer, Science 267 (1995) 1947–1953.
[2] W.L. Johnson, MRS Bull. 24 (1999) 42–56.
[3] W.H. Wang, C. Dong, C.H. Shek, Mater. Sci. Eng. R 44 (2004) 45–89.
[4] P.S. Steif, F. Spaepen, J.W. Hutchinson, Acta Metall. 30 (1982) 447–455.
[5] H. Bei, S. Xie, E.P. George, Phys. Rev. Lett. 96 (2006) 105503.
[6] J. Pan, Q. Chen, L. Liu, Y. Li, Acta Mater. 59 (2011) 5146–5158.
[7] C.C. Hays, C.P. Kim, W.L. Johnson, Phys. Rev. Lett. 84 (2000) 2901.
[8] D.H. Bae, M.H. Lee, D.H. Kim, D.J. Sordelet, Appl. Phys. Lett. 83 (2003) 2312–2314.
[9] P. Yu, H.Y. Bai, Mater. Sci. Eng. A 485 (2008) 1–4.
[10] K.B. Kim, J. Das, F. Baier, M.B. Tang, W.H. Wang, J. Eckert, Appl. Phys. Lett. 88 (2006) 051911.
[11] W.H. Wang, Prog. Mater Sci. 52 (2007) 540–596.
[12] C.T. Liu, Z.P. Lu, Intermetallics 13 (2005) 415–418.
[13] A. Inoue, Acta Mater. 48 (2000) 279–306.
[14] S.H. Xie, X.R. Zeng, H.X. Qian, J. Alloy. Compd. 480 (2009) L37–L40.
[15] Y.H. Liu, G. Wang, R.J. Wang, M.X. Pan, W.H. Wang, Science 315 (2007) 1385–1388.
[16] P. Gong, K.F. Yao, Y. Shao, J. Alloy. Compd. 536 (2012) 26–29.
[17] G.Z. Ma, B.A. Sun, S. Pauly, K.K. Song, U. Kühn, D. Chen, J. Eckert, Mater. Sci. Eng. A 563 (2013) 112–116.
[18] L.Y. Chen, Z.D. Fu, G.Q. Zhang, X.P. Hao, Q.K. Jiang, X.D. Wang, Q.P. Cao, H. Franz, Y.G. Liu, H.S. Xie, S.L. Zhang, B.Y. Wang, Y.W. Zeng, J.Z. Jiang, Phys. Rev. Lett. 100 (2008) 075501.
[19] A. Inoue, T. Shibata, T. Zhang, Mater. Trans. JIM 36 (1995) 1420–1426.
[20] J.B. Qiang, W. Zhang, G.Q. Xie, A. Inoue, J. Non-Cryst. Solids 354 (2008) 2054–2059.
[21] D. Ma, H. Cao, L. Ding, Y.A. Chang, K.C. Hsieh, Y. Pan, Appl. Phys. Lett. 87 (2005) 171914.
[22] L.Q. Xing, T.C. Hufnagel, J. Eckert, W. Löser, L. Schultz, Appl. Phys. Lett. 77 (2000) 1970–1972.
[23] N. Mattern, U. Kühn, H. Hermann, H. Ehrenberg, J. Neuefeind, J. Eckert, Acta Mater. 50 (2002) 305–314.
[24] Z.P. Lu, H. Tan, Y. Li, S.C. Ng, Scr. Mater. 42 (2000) 667–673.
[25] P.A. Bancel, P.A. Heiney, P.W. Stephens, A.I. Goldman, P.M. Horn, Phys. Rev. Lett. 54 (1985) 2422.